

# Time-resolved study of solvent-induced recombination in photodissociated $\text{IBr}^-(\text{CO}_2)_n$ clusters

Vladimir Dribinski, Jack Barbera, Joshua P. Martin, Annette Svendsen,<sup>a)</sup>  
 Matthew A. Thompson, Robert Parson, and W. Carl Lineberger<sup>b)</sup>  
*JILA, University of Colorado, Boulder, Colorado 80309 and Department of Chemistry and Biochemistry,  
 University of Colorado, Boulder, Colorado 80309*

(Received 17 April 2006; accepted 31 May 2006; published online 3 October 2006)

We report the time-resolved recombination of photodissociated  $\text{IBr}^-(\text{CO}_2)_n$  ( $n=5-10$ ) clusters following excitation to the dissociative  $\text{IBr}^-A' \ ^2\Pi_{1/2}$  state of the chromophore via a 180 fs, 795 nm laser pulse. Dissociation from the  $A'$  state of the bare anion results in  $\text{I}^-$  and  $\text{Br}$  products. Upon solvation with  $\text{CO}_2$ , the  $\text{IBr}^-$  chromophore regains near-IR absorption only after recombination and vibrational relaxation on the ground electronic state. The recombination time was determined by using a delayed femtosecond probe laser, at the same wavelength as the pump, and detecting ionic photoproducts of the recombined  $\text{IBr}^-$  cluster ions. In sharp contrast to previous studies involving solvated  $\text{I}_2^-$ , the observed recombination times for  $\text{IBr}^-(\text{CO}_2)_n$  increase dramatically with increasing cluster size, from 12 ps for  $n=5$  to 900 ps for  $n=8, 10$ . The nanosecond recombination times are especially surprising in that the overall recombination probability for these cluster ions is unity. Over the range of 5–10 solvent molecules, calculations show that the solvent is very asymmetrically distributed, localized around the Br end of the  $\text{IBr}^-$  chromophore. It is proposed that this asymmetric solvation delays the recombination of the dissociating  $\text{IBr}^-$ , in part through a solvent-induced well in the  $A'$  state that (for  $n=8, 10$ ) traps the evolving complex. Extensive electronic structure calculations and nonadiabatic molecular dynamics simulations provide a framework to understand this unexpected behavior. © 2006 American Institute of Physics. [DOI: 10.1063/1.2217741]

## I. INTRODUCTION

The effects of solvation on the course of chemical reactions have long been the subject of major theoretical and experimental interest. However, detailed studies and fundamental understanding of these effects are often hindered by the complexity of the problem that involves large numbers of interacting species along with rapid changes in their configurations.

An alternative approach to gain insight on the nature of these interactions is to look at a simplified problem with a known number of solvent molecules, using gas phase cluster ions. Using supersonic expansion for cluster formation allows one to cluster ions at low temperatures and, therefore, with better-defined initial configurations. In addition, the use of charged clusters makes it easy to select the precursor as well as detect products using simple mass-spectrometry methods. By varying the cluster size, one can balance the feasibility of the problem with the degree of detail to be extracted. The utilization of anions as a tool to probe chemical dynamics is extensively discussed by Neumark<sup>1</sup> in this issue.

Although it may seem surprising that a small cluster can serve as an adequate prototype of a much larger condensed-phase system, it has been demonstrated that certain solvent-induced phenomena require very few solvent molecules to

occur. Examples of such phenomena are the “cage” effect<sup>2–24</sup> and the solvent-induced recombination, which in some cases can be observed with as few as only one solvent molecule present.<sup>25,26</sup>

This paper continues an extensive experimental study of dihalide ion clusters  $XY^-L_n$  ( $X, Y = \text{I}, \text{Br}, \text{Cl}$ ;  $L = \text{CO}_2, \text{OCS}, \text{Ar}$ ) that display the profound effects of the solvent on the dissociation dynamics of the  $XY^-$  core.<sup>26–37</sup> In the present work we investigate dependence of the rate of solvent-induced recombination in size-selected  $\text{IBr}^-(\text{CO}_2)_n$ ,  $n = 5-10$  clusters excited to the  $A' \ ^2\Pi_{1/2}$  state of the  $\text{IBr}^-$  chromophore, as a function of number of solvent molecules. The investigation encompasses a range of solvation where the recombination has been shown to be nearly complete<sup>38</sup> and where past experience<sup>35,37,39,40</sup> indicates the likelihood both of very rapid recombination rates and of rates that increase with increasing solvation.

Potential energy curves of the unsolvated  $\text{IBr}^-$  anion are shown in Fig. 1.<sup>38</sup> Excitation of this unsolvated anion with 790 nm radiation produces only  $\text{I}^-$  and  $\text{Br}$  fragments, indicating that the  $A' \ ^2\Pi$  state is the only state excited at this wavelength. Our earlier investigation of  $\text{IBr}^-$  showed<sup>38</sup> that the addition of a single  $\text{CO}_2$  solvent results in the appearance of the  $\text{Br}^-$  ion, indicating a solvent-induced nonadiabatic process. The first “caged” product,  $\text{IBr}^-$ , appears from excitation of  $\text{IBr}^-(\text{CO}_2)_2$ . The cage fraction rises to 90% for  $\text{IBr}^-(\text{CO}_2)_5$ , and, for clusters with  $n \geq 8$ , only recombined ionic products are detected. This behavior is very similar to that observed for  $\text{I}_2^-(\text{CO}_2)_n$ ,<sup>40</sup> and, consequently, trends in the

<sup>a)</sup>Permanent address: Department of Physics and Astronomy, University of Aarhus, Aarhus, Denmark.

<sup>b)</sup>Electronic mail: wcl@jila.colorado.edu

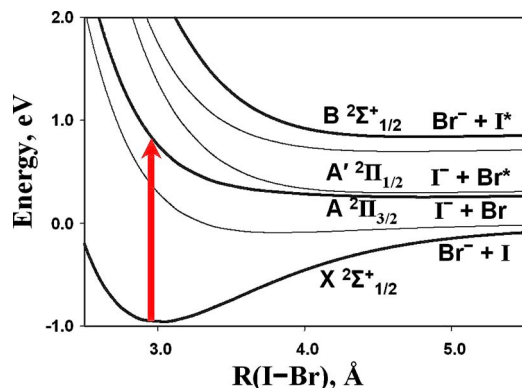


FIG. 1. Calculated potential energy curves for the lowest six electronic states of  $\text{IBr}^-$ . The arrow indicates the pump/probe transition from the ground state ( $X$ ) to the first excited state ( $A'$ ).

time scales of the recombination processes for  $\text{IBr}^-(\text{CO}_2)_n$  and  $\text{I}_2(\text{CO}_2)_n$  were expected to be comparable. However, a preliminary measurement of the recombination time for  $\text{IBr}^-(\text{CO}_2)_8$  found a nanosecond recombination time, some two orders of magnitude slower than that of  $\text{I}_2(\text{CO}_2)_n$  clusters.<sup>38</sup> Such a drastic discrepancy must reflect a fundamental difference between  $\text{IBr}^-(\text{CO}_2)_n$  and  $\text{I}_2(\text{CO}_2)_n$ . In order to help understand this difference, we have carried out a more thorough experimental measurement of recombination times for a number of  $\text{IBr}^-(\text{CO}_2)_n$  clusters. When complemented by extensive calculations,<sup>41</sup> these experiments provide the likely explanation for the anomalous recombination of  $\text{IBr}^-(\text{CO}_2)_n$  as arising from a solvent-induced trap on the  $\text{IBr}^-A' 2\Pi_{1/2}$  surface, a trap that arises from the solvent asymmetry and is deepest for 5–10  $\text{CO}_2$  solvent molecules.

The paper is organized as follows. Section II briefly describes the experimental setup, explains the technique used to determine the recombination times, and outlines the theoretical methods used in determining minimum-energy structures, radial potential energy surfaces (PESs), and molecular dynamics simulations. Section III shows experimental results and their analysis. These results are explained in Sec. IV using a physical picture that is based on the results of *ab initio* calculations and compared to the molecular dynamics simulations. Section V summarizes our experimental findings and suggested explanations.

## II. EXPERIMENTAL AND THEORETICAL METHODOLOGY

### A. Experimental apparatus overview

The experimental apparatus has been described in detail elsewhere,<sup>42</sup> and only a brief description will be given here. The  $\text{IBr}^-(\text{CO}_2)_n$  cluster ions are formed<sup>43</sup> in a supersonic expansion of a gas mixture obtained by passing 2–3 atm of  $\text{CO}_2$  through a glass reservoir containing crystals of  $\text{IBr}$  (Aldrich, 98% purity) at room temperature. The time required to passivate the supply gas line was reduced from a week<sup>38</sup> to less than a day by replacing stainless steel lines with Teflon tubing.<sup>44</sup> The mixture enters a source chamber through the 0.8 mm diameter nozzle of a General Valve operating at 100 Hz repetition rate and is immediately intersected by a 300  $\mu\text{A}$ , 1 keV electron beam. Attachment of slow second-

ary electrons produces  $\text{IBr}^-$ , from which  $\text{IBr}^-(\text{CO}_2)_n$  clusters grow via ion-neutral collisions. Based on prior modeling of the expansion conditions,<sup>45,46</sup> we estimate the resultant cluster ion internal energy to correspond to a temperature of 40–70 K.

After drifting for 20 cm in the expansion, a pulsed electric potential perpendicular to the expansion extracts the ions into a Wiley-McLaren time-of-flight (TOF) mass spectrometer, where they are further accelerated to 2.5 keV and steered into the interaction region, at which point the ion packet is intersected with a collimated pump and delayed probe laser beam with the same wavelength, 797 nm. Secondary mass selection of the ionic photoproducts is performed by a reflectron-type mass spectrometer. Variation of the reflectron voltage allows transmission of either the parent anionic clusters or charged dissociation products.

### B. Laser system

The femtosecond laser pulses are generated by a system that consists of a Coherent Mira 900-B Ti:sapphire oscillator pumped by Coherent Verdi V5 Nd:YVO<sub>4</sub> solid state laser combined with a Quantronix Titan regenerative/multipass Ti:sapphire amplifier pumped by a Quantronix 527 Nd:YLF laser. The output of the amplifier (797 nm, ~180 fs, 3 mJ/pulse) is split into two beams: ~60% of the initial energy is used to excite the parent cluster (pump), while ~40% is used to detect the products (probe). The polarizations of the pump and probe beams are parallel.

The optical path of the pump beam contains a computer-controlled, precision variable delay stage that allows variation of the pump-probe pulse delay over 800 ps, with a time resolution of ~100 fs. The required longer delay times are accomplished by means of a manually adjusted delay in the probe beam path, allowing adjustable delays of up to 3.5 ns with a precision of ~20 ps.

### C. Measurements of the recombination dynamics

The methodology used to determine the recombination dynamics of  $\text{IBr}^-(\text{CO}_2)_n$  clusters after excitation to the  $A' 2\Pi_{1/2}$  state is based on the fact that the dissociated  $\text{IBr}^-$  chromophore regains near-IR absorption only after recombination and substantial vibrational relaxation on the ground electronic surface. Previous studies of  $\text{IBr}^-(\text{CO}_2)_n A' 2\Pi_{1/2}$  photofragmentation<sup>38</sup> demonstrated that, for clusters with  $n \geq 5$ , the recombination efficiency exceeds 90% and is 100% for  $n \geq 8$ . The energy released in the process of bond reformation results in evaporation of 4–6  $\text{CO}_2$  molecules, in accordance with the solvent binding energetics.<sup>38</sup> Therefore, absorption of another photon at the same wavelength by these smaller clusters leads to the formation of distinct secondary products. In order to follow the recombination process, the number of these secondary product ions is monitored as a function of the pump-probe delay time to follow the recombination process. There are considerable background signals present at delay times corresponding to small recombination signals, and these contributions were accounted for by data acquisition sequences that have been previously described in detail.<sup>35,40,46</sup>

TABLE I. One-photon (Ref. 47) (pump only) and expected two-photon (pump/probe) ionic products for selected  $\text{IBr}^-(\text{CO}_2)_n$  clusters, following 790 nm excitation. Only significant ( $>5\%$  of total) secondary products are shown. For each parent cluster size, those secondary products recorded in our experiments and used for determination of recombination time scales are shown in **bold**.

Parent cluster	Primary (one-photon) products	Secondary (two-photon) products
$\text{IBr}^-(\text{CO}_2)_5$	3% $\text{IBr}^-(\text{CO}_2)_2$ 6% $\text{IBr}^-(\text{CO}_2)_3$ 49% $\text{IBr}^-$ 36% $\text{IBr}^-(\text{CO}_2)$ 6% <b><math>\text{IBr}^-(\text{CO}_2)_2</math></b>	<b>69% <math>\text{I}^-</math></b> 28% $\text{I}^-(\text{CO}_2)$ 3% Minor products
$\text{IBr}^-(\text{CO}_2)_6$	4% $\text{Br}^-(\text{CO}_2)_3$ 6% $\text{IBr}^-$ 58% $\text{IBr}^-(\text{CO}_2)$ 30% $\text{IBr}^-(\text{CO}_2)_2$ 2% $\text{IBr}^-(\text{CO}_2)_3$	<b>30% <math>\text{I}^-</math></b> <b>58% <math>\text{I}^-(\text{CO}_2)</math></b> 12% Minor products
$\text{IBr}^-(\text{CO}_2)_7$	3% $\text{Br}^-(\text{CO}_2)_4$ 16% $\text{IBr}^-(\text{CO}_2)$ 51% $\text{IBr}^-(\text{CO}_2)_2$ 22% $\text{IBr}^-(\text{CO}_2)_3$ 8% $\text{IBr}^-(\text{CO}_2)_4$	<b>9% <math>\text{I}^-</math></b> <b>55% <math>\text{I}^-(\text{CO}_2)</math></b> <b>10% <math>\text{Br}^-(\text{CO}_2)</math></b> 16% $\text{IBr}^-$ 10% Minor products
$\text{IBr}^-(\text{CO}_2)_8$	2% $\text{IBr}^-(\text{CO}_2)$ 26% $\text{IBr}^-(\text{CO}_2)_2$ 49% $\text{IBr}^-(\text{CO}_2)_3$ 20% $\text{IBr}^-(\text{CO}_2)_4$ 3% $\text{IBr}^-(\text{CO}_2)_5$	<b>42% <math>\text{I}^-(\text{CO}_2)</math></b> <b>11% <math>\text{Br}^-(\text{CO}_2)</math></b> <b>30% <math>\text{IBr}^-</math></b> 17% Minor products
$\text{IBr}^-(\text{CO}_2)_{10}$	12% $\text{IBr}^-(\text{CO}_2)_3$ 38% $\text{IBr}^-(\text{CO}_2)_4$ 38% $\text{IBr}^-(\text{CO}_2)_5$ 12% $\text{IBr}^-(\text{CO}_2)_6$	7% $\text{I}^-(\text{CO}_2)$ 8% $\text{Br}^-(\text{CO}_2)_2$ <b>50% <math>\text{IBr}^-</math></b> <b>21% <math>\text{IBr}^-(\text{CO}_2)</math></b> 6% $\text{IBr}^-(\text{CO}_2)_2$ 8% Minor products

The expected distribution of pump-probe product ions was obtained from sequential application of the measured<sup>38,47</sup> distribution of one-photon ionic photoproducts and is summarized in Table I. The observed secondary product branching ratios differ only slightly from the ratios reported in Table I. This, however, should be expected, since the one-photon products used to estimate the two-photon ratios were obtained at cluster temperatures of 40–70 K.<sup>47</sup> While parent clusters in our experiments are expected to have similar temperatures, the internal energy of the recombined products may be substantially higher leading to variation in the number of solvent molecules evaporated. As the product ions are mass selected, it is possible to obtain potentially different recombination signals from each secondary product ion, as has previously been observed.<sup>37</sup> In the present studies, the time dependence of several different secondary products arising from a single parent ion was investigated, and no substantial differences were detected. Consequently, the time-dependent data for each parent ion reported in the next section arise from the sum of those most intense secondary two-photon products that are shown in boldface in Table I.

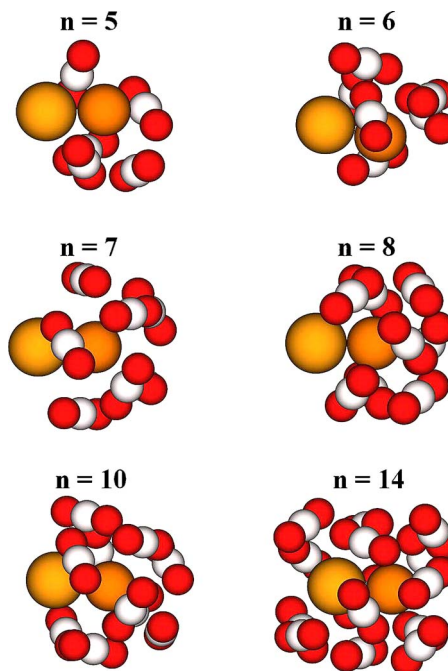


FIG. 2. Minimum-energy structures of  $\text{IBr}^-$  with various numbers of  $\text{CO}_2$  solvent molecules, indicating asymmetric solvation around Br end.

## D. Theoretical methods

The  $\text{IBr}^-$  potential energy surface and associated electronic properties needed for the molecular dynamics (MD) simulations were obtained using MOLPRO 2002.6.<sup>48</sup> The energy-consistent effective core potential (ECP) of the Stuttgart-Bonn group<sup>49</sup> was used; specifically, we employed large-core MDF ECPs based upon multi-configuration Dirac-Hartree-Fock calculations of the neutral atom. This potential also includes a core polarization potential that models the charge-induced dipole interaction of the core. The basis sets used are an augmented form  $(7s7p3d2f)/[5s5p3d2f]$  of the stock  $(6s6p)/[4s4p]$  basis sets included with the ECPnMDF ECPs.<sup>49,50</sup> These calculations used the internally-contracted multi-reference configuration interaction methods developed by Knowles and Werner.<sup>51–53</sup> The reference orbitals and configurations were obtained from state averaged complete active-space self-consistent field calculations<sup>54,55</sup> that consisted of the 15 electrons in the lowest two  $\Sigma$ ,  $\Pi_x$ , and  $\Pi_y$  states that arise from the  $^2P$  and  $^1S$  states of the separated atomic components. A spin-orbit calculation of all six states was then performed using spin-orbit ECPs.<sup>56</sup> This was performed at 42 points along the PES corresponding to bond lengths ranging from 4.5 to  $100a_0$ .

The minimum-energy  $\text{IBr}^-(\text{CO}_2)_n$  structures were constructed by sampling 201 configurations from a 1 ns trajectory on the  $\text{IBr}^-(\text{CO}_2)_n$  ground state having an average temperature of 80 K. These configurations were then quenched to local minima using Newton-Raphson minimization.<sup>57</sup> A sample of the resulting minimum-energy structures for relevant numbers of solvent molecules is presented in Fig. 2. The solvent asymmetry that leads to strong modification of the  $\text{IBr}^-$  electronic states is readily seen.

In order to more quantitatively investigate the effect of the solvent molecules on the  $\text{IBr}^-$  potential curves (Fig. 1),

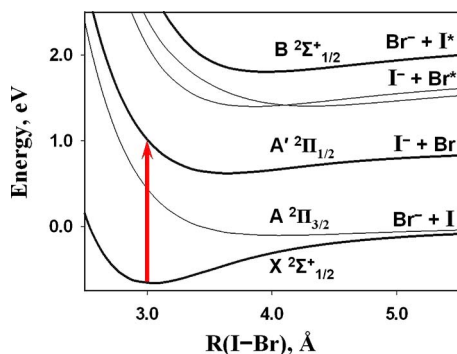


FIG. 3. Calculated potential energy curves for the lowest six electronic states of  $\text{IBr}^-(\text{CO}_2)_8$ . The arrow indicates the pump/probe transition from the ground state (X) to the first excited state (A').

the  $\text{IBr}^-(\text{CO}_2)_8$  minimum-energy structure was used to construct a radial cut through the  $\text{IBr}^-(\text{CO}_2)_8$  potential energy surface (Fig. 3) using the MD program described below. To generate the potential plot (Fig. 3), the iodine atom is “pulled” away from the minimum-energy configuration of  $\text{IBr}^-(\text{CO}_2)_8$ , and the energies of the six spin-orbit states are obtained as a function of the I–Br distance with the solvent fixed at initial configuration. This slice through the  $\text{IBr}^-(\text{CO}_2)_8$  surface can rapidly change with solvent configuration.

The MD simulations for  $\text{IBr}^-(\text{CO}_2)_n$  are based on the effective Hamiltonian method developed by Maslen *et al.*<sup>58</sup> previously applied to  $\text{I}_2^-(\text{CO}_2)_n$ .<sup>59–64</sup> Briefly, the  $\text{IBr}^-$ – $\text{CO}_2$  interaction is based on an operator including electrostatic and induction terms for the solute and solvent. For the solute, distributed multipole analysis<sup>65</sup> (DMA) is performed during the *ab initio* calculations detailed above. More importantly, transition DMA is performed which allows for calculation of the polarization response of the solute to the solvent. The solvent charge distribution and polarization are based on a condensed-phase model.<sup>66</sup> The short-range dispersion-repulsion interactions are described by atom-atom Lennard-Jones potentials based on high resolution photoelectron spectra<sup>67</sup> and from fits of CR-CCSD[T] calculations performed in GAMESS (Refs. 68 and 69) of  $\text{Br}^- \cdots \text{CO}_2$ . At each time step in the simulation, the Hamiltonian is diagonalized to yield the energies, forces, and nonadiabatic transition probabilities needed for the next step. On a single state, motion is computed using the velocity Verlet algorithm,<sup>70</sup> while nonadiabatic transitions are performed according to a modified<sup>60</sup> version of Tully’s surface-hopping method.<sup>71,72</sup>

### III. RESULTS AND ANALYSIS

The only previous measurement of the recombination time in  $\text{IBr}^-(\text{CO}_2)_n$  was conducted for the  $n=8$  cluster.<sup>38</sup> Although no well-defined time dependence was recorded in that study, unambiguous evidence for recombination on a nanosecond scale was obtained. This finding was different from our expectation of rapid, picosecond-scale recombination based on studies of the similar  $\text{I}_2^-(\text{CO}_2)_n$  system, in which the recombination times decreased from 16 to 5 ps as the cluster size increased from  $n=8$  to  $n=17$ .<sup>35,37,40,73</sup>

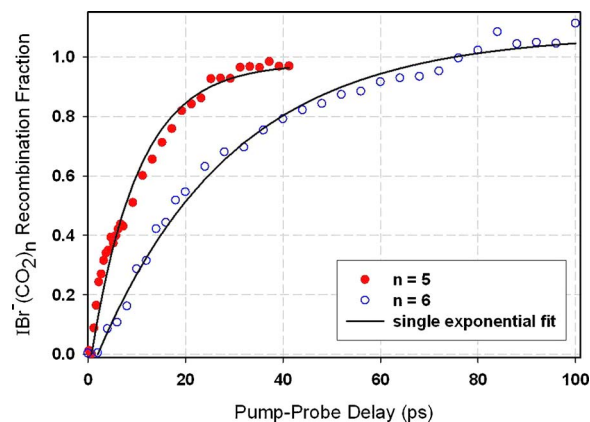


FIG. 4. The  $\text{IBr}^-(\text{CO}_2)_5$  (closed circle) and  $\text{IBr}^-(\text{CO}_2)_6$  (open circle) recombination fractions as a function of time following excitation to the  $A'$  state. Solid lines represent single-exponential fits which yield recombination times of  $12 \pm 0.5$  ps ( $n=5$ ) and  $30 \pm 5$  ps ( $n=6$ ).

Figure 4 shows time-dependent pump/probe signal obtained from the excitation of  $\text{IBr}^-(\text{CO}_2)_5$  and  $\text{IBr}^-(\text{CO}_2)_6$  at 797 nm. It is immediately apparent that the absorption recovery time is much shorter than that previously observed for the larger  $\text{IBr}^-(\text{CO}_2)_8$  anion. In addition, the recovery time increases with additional solvation, in marked contrast to our previous experience.<sup>35,37,40,73</sup> Over the 100 ps time shown in this figure, there appears to be a simple functional form to the recovery, and we could fit the data to the single-exponential form

$$N(t) = [1 - e^{-t/\tau}],$$

with a high-quality fit and with no statistical indications for the necessity to include a second time constant. The resulting fits yield recovery times ( $\tau$ ) of  $12 \pm 0.5$  and  $30 \pm 5$  ps for  $\text{IBr}^-(\text{CO}_2)_5$  and  $\text{IBr}^-(\text{CO}_2)_6$ , respectively, and are displayed as solid lines in Fig. 4. Unlike the previously obtained value for  $\text{IBr}^-(\text{CO}_2)_8$ ,<sup>38</sup> the magnitude of these times is in qualitative agreement with those measured previously for  $\text{I}_2^-(\text{CO}_2)_n$  recombination,<sup>35,37,40,73</sup> although the cluster size dependence is opposite to that observed for  $\text{I}_2^-(\text{CO}_2)_n$ .

An interesting observation is emphasized in Fig. 5,

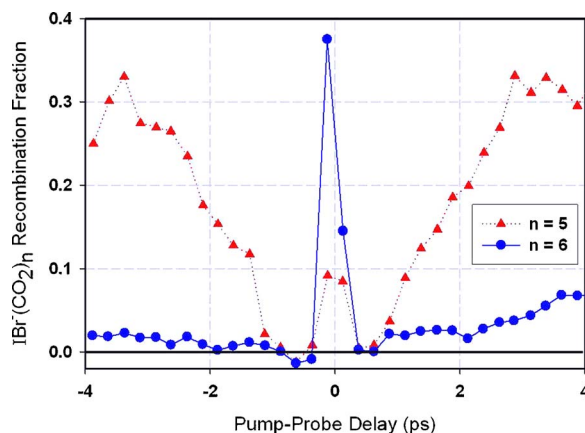


FIG. 5. Short time recombination fractions of  $\text{IBr}^-(\text{CO}_2)_5$  (triangle) and  $\text{IBr}^-(\text{CO}_2)_6$  (circle) showing symmetry in data due to identical pump/probe wavelengths. Coherence peak at  $t=0$  due to enhancement of two-photon background. Rising signal delayed by  $\sim 0.7$  ps ( $n=5$ ) and  $\sim 2$  ps ( $n=6$ ).

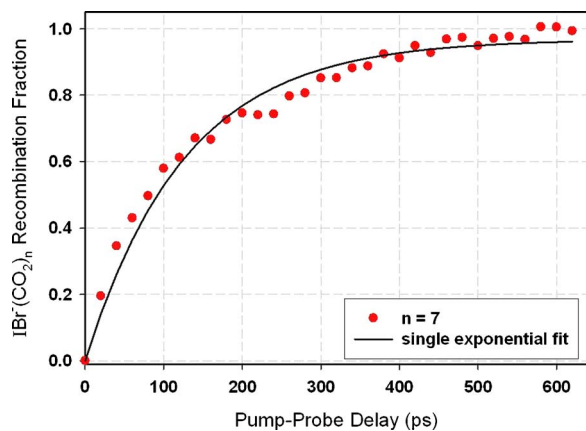


FIG. 6. The  $\text{IBr}^-(\text{CO}_2)_7$  recombination fraction as a function of time following excitation to the  $A'$  state. The solid line represents a single-exponential fit which yields a recombination time of  $140 \pm 20$  ps.

where more detailed recombination signals at early times are presented. One can see that there is a noticeable delay in the appearance of time-dependent signal. For  $n=5$  this delay is  $\sim 0.7$  ps while for  $n=6$  it is  $\sim 2$  ps. One consequence of the long recovery times observed for the larger clusters is that the very low recombination signals at early times preclude our conclusion that this delayed onset persists to larger cluster ions. However, there is no *a priori* reason to expect otherwise.

Due to the fact that both pump and probe laser pulses have the same wavelengths and comparable energies, the pump/probe signal in our experiment must have a symmetric shape about  $t=0$ , although the unequal pump and probe intensities mean that the intensity for some  $t < 0$  can be different from the corresponding  $t > 0$  signal. Moreover, since time-independent background results from the two-photon absorption of either pump or probe radiation alone, this background doubles when pump and probe pulses overlap in time giving rise to a “coherence peak.” This peak is used to determine the exact location of  $t=0$ .

As more  $\text{CO}_2$  solvent molecules are added we obtain longer recombination times, in contrast to those measured for  $\text{I}_2^-(\text{CO}_2)_n$ .<sup>35,37,40,73</sup> The addition of just one more solvent molecule to  $\text{IBr}^-(\text{CO}_2)_6$  results in a very large change in the recombination time scale. Figure 6 shows the absorption recovery signal for  $\text{IBr}^-(\text{CO}_2)_7$ . A single-exponential fit of these data gives a time constant of  $140 \pm 20$  ps. Increasing the cluster size to  $n=8$  and  $n=10$  results in slower recombination times. Figure 7 shows a single-exponential fit for  $n=8$  and  $n=10$ . Both cluster size sets are equally well represented by the same single-exponential rise. This fit yields a recombination time of  $900 \pm 300$  ps, in good agreement with the previous estimate for  $n=8$ .<sup>38</sup> Due to very low intensity of the  $\text{IBr}^-(\text{CO}_2)_{10}$  parent cluster, the corresponding pump/probe signal is noisier than that of  $\text{IBr}^-(\text{CO}_2)_8$ . Attempts to obtain adequate intensities of larger clusters were, unfortunately, unsuccessful. As the behavior of these larger cluster ions would be an important test of the predictions of the simulations, we hope to be able soon to modify the ion source to afford production of larger cluster ions.

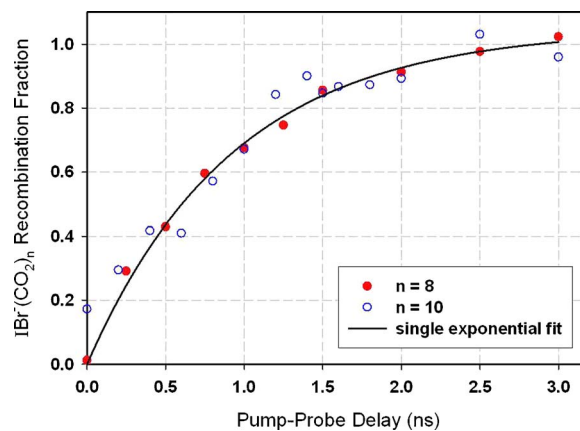


FIG. 7. The  $\text{IBr}^-(\text{CO}_2)_8$  (closed circle) and  $\text{IBr}^-(\text{CO}_2)_{10}$  (open circle) recombination fractions as a function of time following excitation to the  $A'$  state. The solid line represents a single-exponential fit which nicely describes both data sets and yields a recombination time of  $900 \pm 100$  ps. The  $n=10$  data exhibit more noise due to very low ion signals.

#### IV. DISCUSSION

The experimental results obtained in this study and presented in previous sections can be rationalized using a physical picture based on calculations<sup>41</sup> and on comparisons to similar  $\text{I}_2^-(\text{CO}_2)_n$  and  $\text{ICl}^-(\text{CO}_2)_n$  systems.<sup>26,40</sup> According to *ab initio* calculations and other experimental investigations, there is a major qualitative difference between the shape of the  $A'$   ${}^2\Pi_{1/2}$  curve in  $\text{I}_2^-$  (Refs. 33–35 and 37) and those in  $\text{IBr}^-$  (Ref. 41) and  $\text{ICl}^-$ .<sup>26</sup> While the  $A'$  state of  $\text{I}_2^-$  is essentially repulsive,<sup>74</sup> the corresponding state of  $\text{IBr}^-$  exhibits a detectable well<sup>75</sup> at an internuclear separation of  $\sim 4.5$ – $5$  Å (see Fig. 1). Addition of asymmetrically placed solvent molecules increases the depth of this well until it reaches a maximum depth for  $\text{IBr}^-(\text{CO}_2)_8$  and changes its radial location (Fig. 3). According to our structure calculations, this is the most asymmetric solvent configuration, based on the solvent electric field at the center of the solute ion. In this solvent size range, the well depth is comparable to the binding energy of a single solvent molecule and could readily slow the evaporative cooling process, the mechanism whereby the recombined solute anion returns to near its initial energy. We will argue that this well is responsible for “trapping” the  $\text{IBr}^-$  solute on the  $A'$  surface and leads to the slow recombination observed over a small range of partial solvation.

Nonadiabatic MD simulations of  $\text{IBr}^-(\text{CO}_2)_{5-13}$  were carried out to obtain the time dependence for the recombination process described above. All simulations used a time step of 1 fs, while the length of simulations ranged from 20 ps for  $\text{IBr}^-(\text{CO}_2)_5$  to 2000 ps for  $\text{IBr}^-(\text{CO}_2)_{10}$ , with ensemble sizes ranging from 35 trajectories for  $\text{IBr}^-(\text{CO}_2)_{10}$  to over 1700 for  $\text{IBr}^-(\text{CO}_2)_5$ . The ensembles of trajectories gave no indication for the necessity of a fitting form more complicated than the simple exponential form employed to fit the experimental data. Consequently, the MD simulations were summarized by a functional form consisting of a single-exponential fit to the fraction of total recombined trajectories over time. The resulting time constants increased rapidly with increasing solvation, from 5 ps for  $\text{IBr}^-(\text{CO}_2)_5$  to 5000 ps for  $\text{IBr}^-(\text{CO}_2)_{10}$ . For  $\text{IBr}^-(\text{CO}_2)_{10}$ , only ten recom-

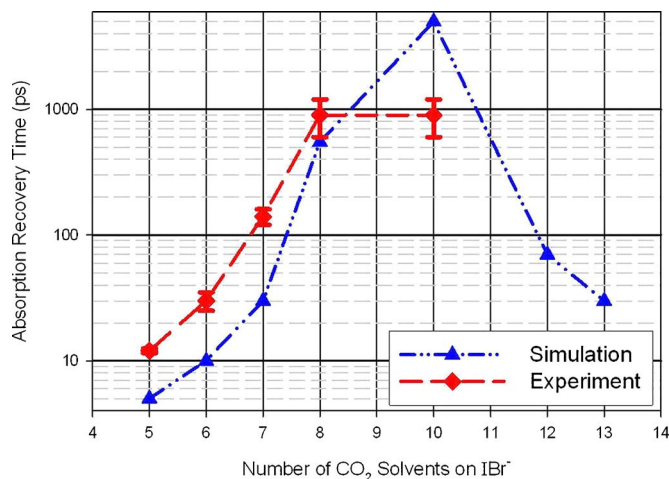


FIG. 8. Comparison of absorption recovery times for experiment (closed diamond) and molecular dynamics simulations (closed triangle). Dashed lines are provided to guide the eye.

bination events were observed in 2 ns for an ensemble of 35 trajectories. Due to the substantial calculation time required, these 35 trajectories were not propagated beyond 2 ns. The reported  $5000 \pm 1000$  ps recombination time constant was obtained by augmenting the simulation data with the experimental observation<sup>38</sup> that all of the photoexcited  $\text{IBr}^-(\text{CO}_2)_{10}$  ions eventually return to the ground state surface, providing an unambiguous long time asymptote for the fit. As the number of solvent molecules is further increased, the recombination time constants dramatically shorten, with  $\text{IBr}^-(\text{CO}_2)_{12}$  showing 70 ps recovery and  $\text{IBr}^-(\text{CO}_2)_{13}$  showing a 30 ps recovery time!

More detailed inspection of the individual trajectories in the MD simulations supports this mechanism of trapping on the  $A'$  excited state. The long recombination times appear to arise from the presence of a configurational transition state, where achieving a narrow range of solvent and solute geometry is necessary for nonadiabatic transition to the ground electronic state of the solute. The results of molecular dynamic simulations are shown in Fig. 8 in comparison to the experimental results. Although the simulations produce faster recombination times than those measured, by a factor of 3–5, they are in excellent qualitative agreement with experiment, with the exception of  $n=10$ . The magnitude of the experimental error bars in Fig. 8 reflects the range of recombination times observed for each cluster size. The details of the simulations and the nature of the solvent-induced excited state trap will be explored more deeply in a future publication.<sup>41</sup>

Finally, the simulations suggest that for clusters with  $n \geq 12$  recombination time becomes short again (see  $n=12, 13$  in Fig. 8). Experiments are currently underway to confirm this prediction. This would provide an important proof for the physical picture described in this section. The main challenge of the current experiment is the production of sufficient amounts of  $\text{IBr}^-(\text{CO}_2)_{n \geq 10}$  clusters.

In addition to the qualitative agreement between theoretical and experimental time scales, the simulations for clusters with 5 and 6  $\text{CO}_2$  molecules also display initial delays in product appearance similar to those observed in Fig. 5. Al-

though the exact origin of these delays is not completely clear, we assume that they reflect the time required for dissociation, nonadiabatic relaxation to the ground state, and partial vibrational relaxation, all in the absence of an excited state trap.

## V. SUMMARY

Time-resolved experimental studies of the recombination of size-selected  $\text{IBr}^-(\text{CO}_2)_n$  anionic clusters following excitation to the  $A' \ ^2\Pi_{1/2}$  state were carried out using tandem time-of-flight mass spectrometry combined with an ultrafast laser system. The  $\text{IBr}^-$  chromophore near-IR absorption recovery was observed and the time scales of the recombination were extracted from the experimental data. Recombination time scales exhibit very strong dependence on the number of solvent molecules. For clusters with  $n=5-7$ , recombination occurs on a picosecond time scale, similar to that of  $\text{I}_2^-(\text{CO}_2)_n$  clusters. Clusters with 8 and 10  $\text{CO}_2$  molecules exhibit strikingly longer nanosecond time scales. Such changes in the recombination rates are explained in terms of the solvent-induced potential well that is especially deep for configurations involving solvent surrounding primarily the Br atom. Molecular dynamics simulations confirm this picture and are in excellent qualitative agreement with experimental data. The simulations predict an increase of the recombination rate for larger  $\text{IBr}^-(\text{CO}_2)_n$  ( $n > 12$ ) cluster ions; experiments are currently in progress to test this conclusion.

## ACKNOWLEDGMENTS

This work has been supported by the National Science Foundation (CHE051288 and PHY0096822) and the Air Force Office of Scientific Research (FA9550-06-1-006). One of the authors (A.S.) is a 2005 JILA visiting student.

- <sup>1</sup>D. M. Neumark, J. Chem. Phys. **125**, 1 (2006).
- <sup>2</sup>N. A. Abul-Haj and D. F. Kelley, Chem. Phys. Lett. **119**, 182 (1985).
- <sup>3</sup>P. Bado, C. Dupuy, D. Magde, K. R. Wilson, and M. M. Malley, J. Chem. Phys. **80**, 5531 (1984).
- <sup>4</sup>P. B. Beeken, E. A. Hanson, and G. W. Flynn, J. Chem. Phys. **78**, 5892 (1983).
- <sup>5</sup>D. Booth and R. M. Noyes, J. Am. Chem. Soc. **82**, 1868 (1960).
- <sup>6</sup>P. S. Dardi and J. S. Dahler, J. Chem. Phys. **93**, 242 (1990).
- <sup>7</sup>J. Franck and E. Rabinowitch, Trans. Faraday Soc. **30**, 120 (1934).
- <sup>8</sup>A. L. Harris, M. Berg, and C. B. Harris, J. Chem. Phys. **84**, 788 (1986).
- <sup>9</sup>H. Hippler, K. Luther, and J. Troe, Chem. Phys. Lett. **16**, 174 (1972).
- <sup>10</sup>H. Hippler, V. Schubert, and J. Troe, J. Chem. Phys. **81**, 3931 (1984).
- <sup>11</sup>A. E. Johnson, N. E. Levinger, and P. F. Barbara, J. Phys. Chem. **96**, 7841 (1992).
- <sup>12</sup>D. A. V. Kliner, J. C. Alfano, and P. F. Barbara, J. Chem. Phys. **98**, 5375 (1993).
- <sup>13</sup>H. Kunz, J. G. McCaffrey, R. Schriever, and N. Schwentner, J. Chem. Phys. **94**, 1039 (1991).
- <sup>14</sup>Q. Liu, J. K. Wang, and A. H. Zewail, Nature (London) **364**, 427 (1993).
- <sup>15</sup>K. Luther, J. Schroeder, J. Troe, and U. Unterberg, J. Phys. Chem. **84**, 3072 (1980).
- <sup>16</sup>K. Luther and J. Troe, Chem. Phys. Lett. **24**, 85 (1974).
- <sup>17</sup>J. G. McCaffrey, H. Kunz, and N. Schwentner, J. Chem. Phys. **96**, 2825 (1992).
- <sup>18</sup>D. J. Nesbitt and J. T. Hynes, J. Chem. Phys. **77**, 2130 (1982).
- <sup>19</sup>E. D. Potter, Q. Liu, and A. H. Zewail, Chem. Phys. Lett. **200**, 605 (1992).
- <sup>20</sup>E. Rabinowitch and W. C. Wood, Trans. Faraday Soc. **32**, 547 (1936).
- <sup>21</sup>E. Rabinowitch and W. C. Wood, Trans. Faraday Soc. **32**, 1381 (1936).
- <sup>22</sup>G. N. R. Tripathi, R. H. Schuler, and R. W. Fessenden, Chem. Phys. Lett.

- 113**, 563 (1985).
- <sup>23</sup>R. Zadoyan, Z. Li, P. Ashjian, C. C. Martens, and V. A. Apkarian, *Chem. Phys. Lett.* **218**, 504 (1994).
- <sup>24</sup>R. Zadoyan, Z. Li, C. C. Martens, and V. A. Apkarian, *J. Chem. Phys.* **101**, 6648 (1994).
- <sup>25</sup>R. E. Smalley, D. H. Levy, and L. Wharton, *J. Chem. Phys.* **64**, 3266 (1976).
- <sup>26</sup>M. E. Nadal, P. D. Kleiber, and W. C. Lineberger, *J. Chem. Phys.* **105**, 504 (1996).
- <sup>27</sup>B. J. Greenblatt, M. T. Zanni, and D. M. Neumark, *Chem. Phys. Lett.* **258**, 523 (1996).
- <sup>28</sup>M. T. Zanni, T. R. Taylor, B. J. Greenblatt, B. Soep, and D. M. Neumark, *J. Chem. Phys.* **107**, 7613 (1997).
- <sup>29</sup>A. V. Davis, R. Wester, A. E. Bragg, and D. M. Neumark, *J. Chem. Phys.* **119**, 2020 (2003).
- <sup>30</sup>A. V. Davis, M. T. Zanni, C. Frischkorn, M. Elhanine, and D. M. Neumark, *J. Electron Spectrosc. Relat. Phenom.* **112**, 221 (2000).
- <sup>31</sup>B. J. Greenblatt, M. T. Zanni, and D. M. Neumark, *Science* **276**, 1675 (1997).
- <sup>32</sup>B. J. Greenblatt, M. T. Zanni, and D. M. Neumark, *J. Chem. Phys.* **112**, 601 (2000).
- <sup>33</sup>S. Nandi, A. Sanov, N. Delaney, J. Faeder, R. Parson, and W. C. Lineberger, *J. Phys. Chem.* **102**, 8827 (1998).
- <sup>34</sup>J. M. Papanikolas, J. R. Gord, N. E. Levinger, D. Ray, V. Vorsa, and W. C. Lineberger, *J. Phys. Chem.* **95**, 8028 (1991).
- <sup>35</sup>J. M. Papanikolas, V. Vorsa, M. E. Nadal, P. J. Campagnola, H. K. Buchenau, and W. C. Lineberger, *J. Chem. Phys.* **99**, 8733 (1993).
- <sup>36</sup>A. Sanov, T. Sanford, L. J. Butler, J. Vala, R. Kosloff, and W. C. Lineberger, *J. Phys. Chem. A* **103**, 10244 (1999).
- <sup>37</sup>V. Vorsa, S. Nandi, P. J. Campagnola, M. Larsson, and W. C. Lineberger, *J. Chem. Phys.* **106**, 1402 (1997).
- <sup>38</sup>T. Sanford, S.-Y. Han, M. A. Thompson, R. Parson, and W. C. Lineberger, *J. Chem. Phys.* **122**, 054307 (2005).
- <sup>39</sup>A. Sanov and W. C. Lineberger, *Phys. Chem. Chem. Phys.* **6**, 2018 (2004).
- <sup>40</sup>A. Sanov, T. Sanford, S. Nandi, and W. C. Lineberger, *J. Chem. Phys.* **111**, 664 (1999).
- <sup>41</sup>M. A. Thompson and R. Parson (unpublished).
- <sup>42</sup>D. W. Boo, Y. Ozaki, L. H. Andersen, and W. C. Lineberger, *J. Phys. Chem. A* **101**, 6688 (1997).
- <sup>43</sup>M. A. Johnson and W. C. Lineberger, in *Techniques for the Study of Ion Molecule Reactions*, edited by J. M. Farrar and J. W. Saunders (Wiley, New York, 1988), p. 591.
- <sup>44</sup>E. Wrede, S. Laubach, S. Schulenburg, A. Brown, E. R. Wouters, A. J. Orr-Ewing, and M. N. R. Ashfold, *J. Chem. Phys.* **114**, 2629 (2001).
- <sup>45</sup>N. E. Levinger, D. Ray, M. L. Alexander, and W. C. Lineberger, *J. Chem. Phys.* **89**, 5654 (1988).
- <sup>46</sup>V. Vorsa, P. J. Campagnola, S. Nandi, M. Larsson, and W. C. Lineberger, *J. Chem. Phys.* **105**, 2298 (1996).
- <sup>47</sup>T. Sanford, Ph.D. thesis, University of Colorado, 2004.
- <sup>48</sup>H. J. Werner, P. J. Knowles, R. Lindh *et al.*, MOLPRO, version 2002.6, a package of *ab initio* programs, 2003.
- <sup>49</sup>H. Stoll, B. Metz, and M. Dolg, *J. Comput. Chem.* **23**, 767 (2002).
- <sup>50</sup>H. Stoll (private communication).
- <sup>51</sup>H.-J. Werner and P. J. Knowles, *J. Chem. Phys.* **89**, 5803 (1988).
- <sup>52</sup>P. J. Knowles and H. J. Werner, *Theor. Chim. Acta* **84**, 95 (1992).
- <sup>53</sup>P. J. Knowles and H. J. Werner, *Chem. Phys. Lett.* **145**, 514 (1988).
- <sup>54</sup>H. J. Werner and P. J. Knowles, *J. Chem. Phys.* **82**, 5053 (1985).
- <sup>55</sup>P. J. Knowles and H. J. Werner, *Chem. Phys. Lett.* **115**, 259 (1985).
- <sup>56</sup>A. Berning, M. Schweizer, H. J. Werner, P. J. Knowles, and P. Palmieri, *Mol. Phys.* **98**, 1823 (2000).
- <sup>57</sup>W. Press, S. Teukolsky, W. T. Vetterling, and B. P. Flannery, *Numerical Recipes in C: The Art of Scientific Computing*, 2nd ed. (Cambridge University Press, New York, 1992).
- <sup>58</sup>P. E. Maslen, J. Faeder, and R. Parson, *Mol. Phys.* **94**, 693 (1998).
- <sup>59</sup>R. Parson, J. Faeder, and N. Delaney, *J. Phys. Chem. A* **104**, 9653 (2000).
- <sup>60</sup>J. Faeder, N. Delaney, P. E. Maslen, and R. Parson, *Chem. Phys.* **239**, 525 (1998).
- <sup>61</sup>J. Faeder, N. Delaney, P. E. Maslen, and R. Parson, *Chem. Phys. Lett.* **270**, 196 (1997).
- <sup>62</sup>N. Delaney, J. Faeder, and R. Parson, *J. Chem. Phys.* **111**, 452 (1999).
- <sup>63</sup>N. Delaney, J. Faeder, and R. Parson, *J. Chem. Phys.* **111**, 651 (1999).
- <sup>64</sup>N. Delaney, J. Faeder, P. E. Maslen, and R. Parson, *J. Phys. Chem. A* **101**, 8147 (1997).
- <sup>65</sup>A. J. Stone, *The Theory of Intermolecular Forces* (Oxford University Press, New York, 1996).
- <sup>66</sup>C. S. Murthy, S. F. Oshea, and I. R. McDonald, *Mol. Phys.* **50**, 531 (1983).
- <sup>67</sup>I. Yourshaw, Y. X. Zhao, and D. M. Neumark, *J. Chem. Phys.* **105**, 351 (1996).
- <sup>68</sup>M. W. Schmidt, K. K. Baldrige, J. A. Boatz *et al.*, *J. Comput. Chem.* **14**, 1347 (1993).
- <sup>69</sup>M. S. Gordon and M. W. Schmidt, in *Theory and Applications of Computational Chemistry: The First Forty Years*, edited by C. Dykstra, G. Frenking, K. S. Kim, and G. E. Scuseria (Elsevier, Amsterdam, 2005).
- <sup>70</sup>H. C. Andersen, *J. Comput. Phys.* **52**, 24 (1983).
- <sup>71</sup>J. C. Tully, *J. Chem. Phys.* **93**, 1061 (1990).
- <sup>72</sup>S. Hammes-Schiffer and J. C. Tully, *J. Chem. Phys.* **101**, 4657 (1994).
- <sup>73</sup>A. Sanov, S. Nandi, and W. C. Lineberger, *J. Chem. Phys.* **108**, 5155 (1998).
- <sup>74</sup>M. T. Zanni, V. S. Batista, B. J. Greenblatt, W. H. Miller, and D. M. Neumark, *J. Chem. Phys.* **110**, 3748 (1999).
- <sup>75</sup>R. Mabbs, K. Pichugin, and A. Sanov, *J. Chem. Phys.* **122**, 174305 (2005).